Attitude Determination of Highly Dynamic Fixed-wing UAVs

Hugo J. Dias Lopes*

Instituto Superior Técnico, Lisbon, Portugal - 2011/09/19

Taking advantage of the recent Micro-Electro-Mechanical Systems (MEMS), the global cost of the Unmanned Aerial Vehicles (UAVs) has been reduced. However, this reduction in size, power and price of the sensors comes at the expense of an increase in accuracy degradation making it more difficult to estimate the attitude of highly dynamic UAVs. Developing an efficient Attitude and Heading Reference System (AHRS) is then imperative where the integration of the Global Positioning System (GPS) and Inertial Navigation System (INS) can provide a more reliable and accurate AHRS.

In this article, the development of GPS/MEMS-INS systems specifically designed for attitude determination of fixed-wing UAVs is attempted and their performance evaluated. Two Extended Kalman Filters (EKF) are developed where the measurements equations are analytically solved in order to avoid the derivation of the Jacobian matrices. The algorithms make use of GPS-derived accelerations and airspeed sensors distinctly. Simulation results show that the attitude of the UAV can be accurately estimated, with maximum error standard deviations rounding one degree. One of the EKFs algorithms was also tested with real flight data and results show a consistent roll, pitch and yaw angles estimation. Comparisons were made with a commercial device (MTi-G Xsens) and the innovation sequences of the EKF algorithm support its reliability.

I Introduction

The Global Positioning System (GPS) and Inertial Navigation System (INS) data fusion is not a new subject and much research has already been carried.[1,2] The INS can provide continuous and reliable navigation determination. However, the main drawback of this system is that its error increases over time. On the other hand, the GPS can be used to correct these errors, as an aiding system, because it provides long-term stability with high accuracy.[3] Thus, this fusion between the GPS and INS strive to achieve the following:[4]

- Acceptable accuracy level with the possibility to keep decent accuracy over time.
- Continuous and reliable navigation determination (e.g., position, velocity and attitude).

The potential uses of Unmanned Aerial Vehicles (UAVs) in the civil industry are extensive.[5] However, in order to become successful, the global cost of the UAVs has to be affordable to the civilian market. This has led to large strides in sensor cost reduction where the advent of the low-cost Micro-Electro-Mechanical Systems (MEMS) accelerometers and gyroscopes took place in the last years.[3,6]

When the final product of the GPS/INS integration algorithm is the attitude solution it is referred to as Attitude and Heading Reference Systems (AHRS).[7] An AHRS can be seen as an integrated sensor system providing roll, pitch and heading angles with the use accelerometers, rate gyros, and magnetometers. With the integration of the GPS as an aiding system, the final outcome can also be called an integrated AHRS/GPS system. Restricted by the weight, size and power, the small UAVs can not carry traditional attitude measurement systems. Consequently, several AHRS structures with GPS/MEMS-INS integration have been investigated, especially making use of a Kalman filter (KF).[1,8,9]

An inexpensive gyro-free attitude determination system that makes use of accelerometers, magnetometers and GPS as primary sensors, has been studied in Ref. 10. Additionally, an algorithm that takes advantage of the relatively accurate GPS L_1 carrier phase measurements to derive the acceleration of the user was developed in Ref. 11. Moreover, GPS-based attitude determination obtained by differencing signals from multiple antennas has also been a research topic, investigated by many researchers, such as in Refs. 12 and 13. An approach that did not make use of inertial sensors was studied in Ref. 14. Instead, a kinematic model of an aircraft along with the GPS position and velocity measurements derived from a single GPS antenna was used to generate a so called *pseudo-attitude*. More recently, *vector matching* algorithms that makes use of the Earth's magnetic and gravity field vectors as observations, and GPS as an aiding system, have been derived and successfully implemented in Ref. 15.

The somewhat disregarded utilization of GPS-derived accelerations in this integration systems is an open research field with plenty of benefits to take advantage.[16,11] Additionally, upon the Kalman Filter implementation, the derivation of the Jacobian matrices for both process and measurement equations is nontrivial in most applications, and quite often leads to significant implementation difficulties. Two

*MSc Aerospace Engineering student. This article represents the extended abstract of his MSc Thesis: *Attitude Determination of Highly Dynamic Fixed-wing UAVs*, October 2011, Instituto Superior Técnico, Lisbon. E-mail: hugo.lopes@ist.utl.pt

approaches in order to overcome this problem will be attempted, by analytically solving the measurements equations. Thus, in this article the performance of an integrated low-cost GPS/MEMS-INS (or GPS/MEMS-AHRS) system specifically designed for highly dynamic fixed-wing UAVs airborne applications is investigated. *One of the derived algorithms will make use of GPS-derived accelerations and the other of airspeed measurements.*

This paper is organized as follows. First, a brief description about the GPS/INS integration topic is provided in the next section. Then, in Section III, the inertial sensors and the GPS are modeled and the attitude estimation EKF algorithms developed. In Section IV the performance of the algorithms are evaluated with simulated and real flight data. Finally, the conclusions are drawn in Section V.

II GPS/INS Integration

This section describes the various types of GPS/INS integration architectures and the one that was chosen to follow during the attitude estimation algorithms derivation. A short presentation about the Extended Kalman Filter is also given.

II.A GPS/INS Integration Architecture

In general, an INS exhibits relatively low noise from second to second, but tends to drift over time. On the other hand, GPS errors are relatively noisy from second to second, but exhibit no long-term drift. Integrating the information from each sensor results in a GPS/INS navigation system (single algorithm) that operates like a drift-free INS. There are further benefits added depending on the level at which the information is combined.[17]

Basically, there are four types of GPS/INS integration architectures: *uncoupled*, *loosely coupled*, *tightly coupled* and *deeply/ultra-tight* integrated configurations. The loosely and tightly coupled architectures are the most commonly implemented methods. In a loosely coupled integration architecture the two navigation systems operate in cascade, where the GPS provides position and velocity measurements to correct the INS estimations. Thus, the GPS receiver needs at least four satellites to compute a navigational solution to be used in the second EKF. On the other hand, the tightly coupled integration makes use of only one KF and results in a better performance in jamming environments or urban areas.[18]

However, due to a more complex integration where the access to the GPS hardware is required and low computational power is available on board of small UAVs, the loosely coupled architecture seems more than adequate. Furthermore, aircraft like fixed-wing UAVs usually fly in open air and the GPS loss of track is not so common as it happens in land vehicles. Flight test experiences have demonstrated that GPS outages during flights are rare and of a short duration.[13] Due to these reasons, the loosely coupled architecture was chosen as GPS/INS integration architecture.

II.B Kalman Filtering

In essence, the Kalman Filter (KF) is a tool that estimates the variables of a wide range of processes, propagating the mean and covariance of the states through time. In this paper specifically, the Kalman filter will receive the measurements from the GPS, gyroscopes, accelerometers and airspeed sensor, filter them and estimate the attitude (roll, pitch and yaw angles) and the biases of the gyroscopes of the UAV. The ongoing KF cycle computation can be summarized as:[19]

The time update projects the current state estimate ahead in time
↑ ↓
The measurement update adjusts the projected estimate by an actual measurement at that time

II.B.1 Extended Kalman Filter

The *extension* of the KF to nonlinear systems and nonlinear observations leads to the Extended Kalman Filter (EKF).[20] The general nonlinear state-space model is given by:

$$\dot{\underline{x}}(t) = \underline{f}\left[\underline{x}(t), \underline{u}(t), t\right] + G\left[\underline{x}(t), t\right]\underline{w}(t), \quad \underline{x}(0) = \underline{x}_0 \tag{1}$$

$$\underline{z}_m(t) = \underline{h}\left[\underline{x}(t), \underline{u}(t), t\right]$$
$$\underline{z}(t_k) = \underline{z}_m(t_k) + \underline{v}(t_k), \quad k = 1, 2, \ldots \tag{2}$$

where $\underline{f}[\cdot]$ is the system (nonlinear) dynamics, $\underline{h}[\cdot]$ is the nonlinear observer equations that relates the states to the measurements, and $G[\cdot]$ the system noise input matrix. The states, measurements and input vectors are given respectively by $\underline{x}(t)$, $\underline{z}(t)$ and $\underline{u}(t)$. For the implementation of the EKF it is assumed that $\underline{f}[\cdot]$ and $\underline{h}[\cdot]$ are continuous and continuously differentiable with respect to all elements of $\underline{x}(t)$ and $\underline{u}(t)$. Additionally, the system and measurements noise vectors are respectively given by $\underline{w}(t)$ and $\underline{v}(t_k)$. They have the following noise characteristics:

$$E\{\underline{w}(t)\} = 0, \quad E\{\underline{w}(t)\underline{w}^T(\tau)\} = Q(t)\delta(t-\tau) \tag{3a}$$

$$E\{\underline{v}(t_i)\} = 0, \quad E\{\underline{v}(t_i)\underline{v}^T(t_j)\} = R(t_i)\delta_{ij} \tag{3b}$$

where Q and R are the process and observation noise covariance matrices, respectively. The EKF steps are then the following[1]:

Time Update (Prediction)

1. *One step ahead state prediction*: for nonlinear systems this can be obtained by integrating the nonlinear state of Eq. (1):

$$\hat{\underline{x}}(k+1|k) = \hat{\underline{x}}(k|k) + \int_{t_k}^{t_{k+1}} \underline{f}(\underline{x}(t|t_k), \underline{u}^*(t), t)\, dt \tag{4}$$

2. *One step ahead error covariance matrix prediction*: the error covariance matrix P is calculated the same way it is for the Kalman filter with the difference of firstly computing the following linearization:

$$F_x(t_k) = \left.\frac{\partial \underline{f}(\underline{x}(t), \underline{u}(t), t)}{\partial \underline{x}(t)}\right|_{\underline{x}(t)=\underline{x}^*(t_k), \underline{u}(t)=\underline{u}^*(t_k)} \tag{5}$$

[1] These steps are adapted to the implementation in this paper and several variations exist.

where $\underline{x}^*(t_k) = \underline{\hat{x}}(k|k)$. Then, after discretization, to get the discrete-time linearized system dynamics $\Phi(k)$ and the discrete-time system noise covariance matrix $Q_d(k)$, the error covariance matrix prediction can be obtained as follows:

$$P(k+1|k) = \Phi(k)P(k|k)\Phi^T(k) + Q_d(k) \tag{6}$$

Measurement Update (Correction)

3. *Kalman gain computation*: before its calculation, linearization of the observer is necessary:

$$H_x(k+1) = \left.\frac{\partial \underline{h}(\underline{x}(t), \underline{u}(t), t)}{\partial \underline{x}}\right|_{\underline{x}(t)=\underline{x}^*(t_{k+1}), \underline{u}(t)=\underline{u}^*(t_{k+1})} \tag{7}$$

where $\underline{x}^*(t_{k+1}) = \underline{\hat{x}}(k+1|k)$. Then,

$$K(k+1) = P(k+1|k)H_x(k+1)^T \left[H_x(k+1)P(k+1|k)H_x(k+1)^T + R(k)\right]^{-1} \tag{8}$$

4. *Update state estimate with new measurements*:

$$\underline{\hat{x}}(k+1|k+1) = \underline{\hat{x}}(k+1|k) + K(k+1)[\underline{z}(k+1) - \underline{h}(\underline{\hat{x}}(k+1|k), \underline{u}^*(k+1))] \tag{9}$$

5. *Update error covariance matrix*:

$$P(k+1|k+1) = [I - K(k+1)H_x(k+1)]\, P(k+1|k) [I - K(k+1)H_x(k+1)]^T + K(k+1)R(k+1)K^T(k+1) \tag{10}$$

The EKF is initialized with $\underline{\hat{x}}(0|0) = \underline{\hat{x}}_0$ and $P(0|0) = P_0$.

II.B.2 Kalman Filter Reliability

In the real world the real states are not available and it is more difficult to verify if the KF's estimated states are reliable. It is possible to verify the Kalman filter performance by using the knowledge about the statistics of the *innovations*. The innovation $\underline{\nu}$ is the difference between the actual observation and the predicted observation:

$$\underline{\nu}(k+1) = \underline{z}(k+1) - H(k+1)\underline{\hat{x}}(k+1|k) \tag{11}$$

It represents the amount of new information introduced in the system by the current measurement. If the innovation sequence has a zero mean white noise characteristic with covariance given by Eq. (12), then the Kalman filter is working properly.[21]

$$\sigma_\nu(k+1) = H(k+1)P(k+1|k)H^T(k+1) + R(k+1) \tag{12}$$

III Modeling

In this section, the measurements provided by the Inertial Measuring Units (IMUs), GPS receiver and airspeed sensor are going to be modeled. After that, the attitude estimation EKF algorithms are derived in two steps: first the development of the process model and then the derivation of two measurements models (one with GPS-derived accelerations and other with airspeed sensor measurements).

III.A Inertial Measuring Units Modeling

The IMUs are affected by various errors that influence their performance. In practice, the accelerometers and gyroscopes are affected by biases and time-varying noise such as:[22] measurement noise, measurement bias, misalignment and scale factor errors. These characteristics have to be modeled in order to design a suitable estimation/integration algorithm. However, manufacturer supplied specification sheets for low-cost MEMS-IMUs rarely provide enough details to completely construct the error models.[23] Thus, all the associated errors of the IMUs can be simplified to:

$$\begin{aligned} A_{x_m} &= A_x + b_{A_x} + \varepsilon_{A_x} \\ A_{y_m} &= A_y + b_{A_y} + \varepsilon_{A_y} \\ A_{z_m} &= A_z + b_{A_z} + \varepsilon_{A_z} \end{aligned} \tag{13}$$

$$\begin{aligned} p_m &= p + b_p + \varepsilon_p \\ q_m &= q + b_q + \varepsilon_q \\ r_m &= r + b_r + \varepsilon_r \end{aligned} \tag{14}$$

where the accelerometers vector $\underline{A}$ and gyroscopes vector $\underline{\omega}$ were split into their three orthogonal components, $\underline{A} = [A_x,\ A_y,\ A_z]^T$ and $\underline{\omega} = [p,\ q,\ r]^T$, respectively. The subscript m refers to a measured quantity. The bias terms $[b_{A_x},\ b_{A_y},\ b_{A_z}]$ of the accelerometers and $[b_p,\ b_q,\ b_r]$ of the gyroscopes include all the constant *null-shifts* biases and bias-drifts. Additionally, the noise terms of the accelerometers and gyroscopes, respectively, $[\varepsilon_{A_x},\ \varepsilon_{A_y},\ \varepsilon_{A_z}]$ and $[\varepsilon_p,\ \varepsilon_q,\ \varepsilon_r]$, are a function of the measurement noise.

Generally, the noise terms ε are modeled as white Gaussian noise and the bias of the accelerometers can be disregarded due to its relative small magnitude and influence compared to the bias of the gyroscopes. Finally, the bias of the gyroscopes are often modeled as a sum of a *null-shift* bias $\underline{b}_0 = [b_{0_p},\ b_{0_q}\ b_{0_r}]^T$, and a bias-drift $\underline{b}_R = [b_{R_p},\ b_{R_q},\ b_{R_r}]^T$.[7] Thus, from Eq. (14) we obtain:

$$\begin{aligned} p_m &= p + b_{0_p} + b_{R_p} + \varepsilon_p \\ q_m &= q + b_{0_q} + b_{R_q} + \varepsilon_q \\ r_m &= r + b_{0_r} + b_{R_r} + \varepsilon_r \end{aligned} \tag{15}$$

The *null-shift* bias is modeled as a random constant that varies from turn-on to turn-on:

$$\dot{\underline{b}}_0 = 0 \tag{16}$$

The bias-drift, representing the in-run bias variation, is commonly modeled as a first-order Gauss-Markov process given by:

$$\dot{\underline{b}}_R = -\frac{1}{\tau_c}\underline{b}_R + \underline{\varepsilon}_{b_R} \tag{17}$$

where τ_c is the correlation time of the process and $\underline{\varepsilon}_{b_R}$ is the associated white Gaussian noise. However, for low-cost MEMS-IMUs these parameters are often not provided by the manufacturer[2]. Thus, the first-order Gauss-Markov process is used to *overbound* the output errors and not necessarily model them exactly. One approach to overcome this lack of sensor information

[2]For instance, the correlation time τ_c is not provided by the device used to obtain the UAV's real data.

is to use a random walk process instead of a Gauss-Markov process:[24]

$$\dot{\underline{b}}_R = \underline{\varepsilon}_{b_R} \tag{18}$$

where the noise term $\underline{\varepsilon}_{b_R}$ incorporates the full noise of the bias-drift. The variance of this white Gaussian noise parameter is then adjusted manually till reasonable results are obtained.

III.B GPS Modeling

A GPS receiver reports new information as a sequence, typically at 1 to 10Hz rate. However, due to limitations imposed by the internal signal processing of the GPS, higher reporting rates do not necessarily mean a better performance.[25] In order to give direction information, the GPS receiver has to move, otherwise there is no way to determine the orientation of the individual GPS antenna. Since the objective is to implement in fixed-wing UAVs, this problem is avoided.

The GPS receiver modeling is now addressed. The focus is on the GPS velocity and derived accelerations.

III.B.1 GPS Velocity Modeling

The GPS velocity of a vehicle can be obtained measuring the *Doppler shift* between the known satellite carrier frequency and the frequency determined at the receiver.[26] This Doppler shift is directly proportional to the velocity of the receiver, along the direction to the satellite, regardless of the distance to this satellite.[27] The accuracy of this type of GPS velocity is usually much higher when compared to the GPS position (and posteriorly differentiation), reaching values better than 0.01m/s.[28] Additionally, the GPS provides a drift-free reference vector for the course orientation of the airplane. It is assumed that the GPS receiver already provides the velocities in the Navigational reference frame $\mathcal{F}_N$. The GPS velocities are defined as:

$$\underline{V}_{GPS} = \begin{bmatrix} u_{GPS} \\ v_{GPS} \\ w_{GPS} \end{bmatrix} \tag{19}$$

For implementation purposes the GPS velocity can be considered an unbiased and drift-free reference vector affected by white Gaussian noise ε. The measured velocities provided by the GPS receiver are then given as:

$$\begin{aligned} u_{GPS_m} &= u_{GPS} + \varepsilon_{u_{GPS}} \\ v_{GPS_m} &= v_{GPS} + \varepsilon_{v_{GPS}} \\ w_{GPS_m} &= w_{GPS} + \varepsilon_{w_{GPS}} \end{aligned} \tag{20}$$

III.B.2 GPS Acceleration Modeling

Acceleration determination is not yet a typical application of the GPS system. Nevertheless, proposed methods for GPS acceleration determination fall in two categories:[16] one is to derive acceleration directly from GPS determined positions (double differentiation) and the other is based on the Doppler shift method differentiation. The latter has several advantages: it does not rely on the precision of the positions obtained by the GPS and the accuracy will not severely degrade with an increase in the sampling rate (e.g., 10Hz or more).

GPS-derived accelerations will be utilized as an absolute attitude reference by using them in conjunction with a 3-axis accelerometer. This technique was already implemented and results show that a GPS receiver can be used to determine the acceleration of a moving vehicle with reasonable accuracy.[16,29] It has been demonstrated that the GPS is able to provide a measurement of vehicle speed that is sufficiently reliable to determine acceleration with an uncertainty under 0.10m/s^2.[30] Advantages in using GPS-derived accelerations arise with these promising results such as: less susceptibilities to the gravity vector, immunity to vibrational disturbances and temperature fluctuations, and unbiased solutions.

When performing a differentiation, attention should be paid to implement some kind of filter to avoid excessive noise on the output due to the high-frequency components. The GPS-derived accelerations $\underline{a}_{GPS}$ will be modeled using finite differences as presented in Eq. (21). Other differentiation methods could be implemented but we would start *losing* track of the highly dynamic characteristics of the UAV.

$$\begin{aligned} a_{GPS_x} &= \frac{u_{GPS_m}(k) - u_{GPS_m}(k-1)}{\Delta t} \\ a_{GPS_y} &= \frac{v_{GPS_m}(k) - v_{GPS_m}(k-1)}{\Delta t} \\ a_{GPS_z} &= \frac{w_{GPS_m}(k) - w_{GPS_m}(k-1)}{\Delta t} \end{aligned} \tag{21}$$

III.C Process Model

Both attitude estimation algorithms make use of the same Process model presented as follows. The nonlinear Equations of Motion (EOM) used to describe the UAV are kinematic in nature and can be found, for instance, in Ref. 31. Since the objective is to estimate the UAV's attitude, the roll ϕ, pitch θ and yaw ψ angles are chosen as state variables. Additionally, due to the previous discussion about the bias(-drift) of the MEMS-gyroscopes, their bias $\underline{b} = [b_p,\ b_q,\ b_r]^T$ are chosen as state variables as well. Thus, the final state vector is:

$$\underline{x} = [\phi,\ \theta,\ \psi,\ b_p,\ b_q,\ b_r]^T \tag{22}$$

The rate of change of the states is given in Eq. (23). Note that the time dependency term t and the subscript R of Eq. (17) were dropped without loss of generality.

$$\dot{\underline{x}} = \begin{cases} \dot{\phi} = p + q\sin\phi\tan\theta + r\cos\phi\tan\theta \\ \dot{\theta} = q\cos\phi - r\sin\phi \\ \dot{\psi} = q\frac{\sin\phi}{\cos\theta} + r\frac{\cos\phi}{\cos\theta} \\ \dot{b}_p = -\frac{1}{\tau}b_p + \varepsilon_{b_p} \\ \dot{b}_q = -\frac{1}{\tau}b_q + \varepsilon_{b_q} \\ \dot{b}_r = -\frac{1}{\tau}b_r + \varepsilon_{b_r} \end{cases} \tag{23}$$

It is presumed that the angular rates $\underline{\omega} = [p,\ q,\ r]^T$ are available, and they form the input vector $\underline{u}$ of the EKF. With Eq. (14) we arrive at the process model of

the EKF given by Eq. (1) with:

$$\underline{f}\left[\underline{x}(t), \underline{u}(t), t\right] = \begin{bmatrix} p_m - b_p + (q_m - b_q)\sin\phi\tan\theta + (r_m - b_r)\cos\phi\tan\theta \\ (q_m - b_q)\cos\phi - (r_m - b_r)\sin\phi \\ (q_m - b_q)\frac{\sin\phi}{\cos\theta} + (r_m - b_r)\frac{\cos\phi}{\cos\theta} \\ -\frac{1}{\tau}b_p \\ -\frac{1}{\tau}b_q \\ -\frac{1}{\tau}b_r \end{bmatrix} \tag{24}$$

$$G\left[\underline{x}(t), t\right] = \begin{bmatrix} -1 & -\sin\phi\tan\theta & -\cos\phi\tan\theta & 0 & 0 & 0 \\ 0 & -\cos\phi & \sin\phi & 0 & 0 & 0 \\ 0 & -\frac{\sin\phi}{\cos\theta} & -\frac{\cos\phi}{\cos\theta} & 0 & 0 & 0 \\ 0 & 0 & 0 & 1 & 0 & 0 \\ 0 & 0 & 0 & 0 & 1 & 0 \\ 0 & 0 & 0 & 0 & 0 & 1 \end{bmatrix} \tag{25}$$

and,

$$\underline{w} = \left[\varepsilon_p,\ \varepsilon_q,\ \varepsilon_r,\ \varepsilon_{b_p},\ \varepsilon_{b_q},\ \varepsilon_{b_r}\right]^T \tag{26}$$

III.D Measurement Model 1

Estimation of the roll ϕ and pitch θ angles of the aircraft can be made by augmenting the accelerometer with GPS-derived accelerations. Additionally, the course of the UAV can be determined by the GPS (North and East) velocities.

The measurements vector $\underline{z}$ will be composed by the three Euler angles, roll ϕ, pitch θ and yaw ψ. Assuming that the sideslip angle $\beta \approx 0$, the yaw angle is given by[3]:

$$\psi \approx \chi \tag{27}$$

where χ is the course angle. Thus, with the previous assumption, the measured yaw angle can be obtained with the GPS velocity components as follows:

$$\psi_m = \arctan\left(\frac{v_{GPS_m}}{u_{GPS_m}}\right) \tag{28}$$

The measurements of the UAV's roll ϕ_m and pitch θ_m angles can be obtained by measuring acceleration in the Body-fixed reference frame $\mathcal{F}_B$ and relating it to the Navigational reference frame $\mathcal{F}_N$. Recall that the output of an accelerometer is a measurement of the difference between the true vehicle acceleration $\underline{a}$ and the gravitational acceleration $\underline{g}$:[16]

$$\underline{f} = \underline{a} - \underline{g} \tag{29}$$

where $\underline{f}$ is the specific force. Under the assumption that the GPS velocities are obtained in inertial space and transforming all the components to Body-fixed reference frame, the measurements of the accelerometers are then equal to the difference between the GPS-derived accelerations and the gravity:[32]

$$\begin{bmatrix} A_x \\ A_y \\ A_z \end{bmatrix}_B = R_{B/N}(\phi,\theta,\psi)\begin{bmatrix} a_{GPS_x} \\ a_{GPS_y} \\ a_{GPS_z} \end{bmatrix}_N - R_{B/N}(\phi,\theta,\psi)\begin{bmatrix} 0 \\ 0 \\ g \end{bmatrix}_N \tag{30}$$

[3] A negligible sideslip is often considered in an aircraft with a fixed rudder and reasonable aerodynamic characteristics.

where the matrix $R_{B/N}(\phi,\theta,\psi)$ is given by:[31]

$$R_{B/N}(\phi,\theta,\psi) = \begin{bmatrix} c_\psi c_\theta & s_\psi c_\theta & -s_\theta \\ c_\psi s_\theta s_\phi - s_\psi c_\phi & c_\psi c_\phi + s_\psi s_\theta s_\phi & c_\theta s_\phi \\ s_\psi s_\phi + c_\psi s_\theta c_\phi & s_\psi s_\theta c_\phi - c_\psi s_\phi & c_\theta c_\phi \end{bmatrix} \tag{31}$$

with $c_{(\cdot)}$, $s_{(\cdot)}$ and $t_{(\cdot)}$ corresponding respectively to $\cos(\cdot)$, $\sin(\cdot)$ and $\tan(\cdot)$.

Rewriting Eq. (30), a *nonlinear measurement model*, with the accelerations from the accelerometers sensors as measurements, is obtained:

$$\begin{aligned} \begin{bmatrix} A_x \\ A_y \\ A_z \end{bmatrix}_B &= R_{B/N}(\phi,\theta)\begin{bmatrix} a_{GPS_x}\cos\psi + a_{GPS_y}\sin\psi \\ -a_{GPS_x}\sin\psi + a_{GPS_y}\cos\psi \\ a_{GPS_z} - g \end{bmatrix} \\ &= \begin{bmatrix} \cos\theta & 0 & -\sin\theta \\ \sin\phi\sin\theta & \cos\phi & \cos\theta\sin\phi \\ \cos\phi\sin\theta & -\sin\phi & \cos\phi\cos\theta \end{bmatrix}\begin{bmatrix} r_x \\ r_y \\ r_z \end{bmatrix} \end{aligned} \tag{32}$$

where the vector $[r_x,\ r_y,\ r_z]^T$ was defined by the above equation and it includes the UAV's GPS-derived accelerations and gravity acceleration already rotated by the yaw angle $\psi = \psi_m$, determined in Eq. (28). Eq. (32) is clearly nonlinear and finding an analytical solution for ϕ and θ would allow us to use all the three Euler angles as *measurements* in the EKF. Thus, solving the first equation of Expression (32) for θ, yields:

$$A_x = r_x\cos\theta - r_z\sin\theta$$

and after some manipulation, the analytical solution for the *measured* pitch angle $\theta_m = \theta$ can be found:

$$\theta_m = \arctan\left(\frac{-r_x r_z \pm A_x\sqrt{r_x^2 + r_z^2 - A_x^2}}{A_x^2 - r_z^2}\right) \tag{33}$$

If the same strategy is taken for the second equation of Expression (32) the analytical solution for the *measured* roll angle $\phi_m = \phi$ can also be found:

$$\begin{aligned} & A_y = r_x\sin\theta\sin\phi + r_y\cos\phi + r_z\cos\theta\sin\phi \\ \Leftrightarrow\quad & A_y = r_\theta\sin\phi + r_y\cos\phi \end{aligned} \tag{34}$$

where the following was defined:

$$r_\theta = r_x\sin\theta + r_z\cos\theta \tag{35}$$

with $\theta = \theta_m$, already determined in Eq. (33). Performing similar manipulations as the ones applied to obtain the θ_m solution, an analytical solution for the roll angle ϕ_m is given by:

$$\phi_m = \arctan\left(\frac{r_\theta r_y \pm A_y\sqrt{r_y^2 + r_\theta^2 - A_y^2}}{A_y^2 - r_\theta^2}\right) \tag{36}$$

Another solution for ϕ_m but using the A_z accelerometer could be obtained by solving the third equation of Expression (32). With the found analytical solutions for the Euler angles, the measurements vector $\underline{z}$ of the EKF finally becomes:

$$\underline{z} = \begin{bmatrix} \phi_m \\ \theta_m \\ \psi_m \end{bmatrix} = \begin{bmatrix} \arctan\left(\frac{r_\theta r_y + A_y\sqrt{r_y^2 + r_\theta^2 - A_y^2}}{A_y^2 - r_\theta^2}\right) \\ \arctan\left(\frac{-r_x r_z - A_x\sqrt{r_x^2 + r_z^2 - A_x^2}}{A_x^2 - r_z^2}\right) \\ \arctan\left(\frac{v_{GPS_m}}{u_{GPS_m}}\right) \end{bmatrix} \tag{37}$$

The measurements vector calculation is performed every time new GPS data is available. The choice between the plus or minus signals on Eqs. (33) and (36) can be decided based on simulation results. The Observation matrix of the Kalman filter becomes linear with these analytical solutions:

$$H(k+1) = [\ I_{3\times3} \mid 0_{3\times3}\ ] \tag{38}$$

The $\underline{z}$ calculation has to be performed in a *cascade* way: first the yaw angle ψ_m is computed, then the pitch angle θ_m and finally, ϕ_m can be obtained.

III.E Measurement Model 2

A second measurement model is now presented. Newton's laws can be used to express the Body-fixed frame accelerations in terms of gravity, angular rates and axial accelerations:

$$\begin{bmatrix} A_x \\ A_y \\ A_z \end{bmatrix}_B = \begin{bmatrix} \dot{u} \\ \dot{v} \\ \dot{w} \end{bmatrix}_B + \begin{bmatrix} p \\ q \\ r \end{bmatrix}_B \times \begin{bmatrix} u \\ v \\ w \end{bmatrix}_B - \begin{bmatrix} -\sin\theta \\ \cos\theta\sin\phi \\ \cos\theta\cos\phi \end{bmatrix} g \tag{39}$$

where all the terms are expressed in the Body-fixed reference frame $\mathcal{F}_B$. This model will additionally presume the availability of airspeed measurements $\underline{V}_a$ related with the body-velocity by:

$$\begin{bmatrix} u \\ v \\ w \end{bmatrix}_B = V_a \begin{bmatrix} \cos\alpha\cos\beta \\ \sin\beta \\ \sin\alpha\cos\beta \end{bmatrix} \tag{40}$$

where α and β are the angle of attack and sideslip angle, respectively. The V_a (True Airspeed) is obtained through an airspeed sensor (modeled as $V_{am} = V_a + \varepsilon_{V_a}$). The following is assumed through the derivation of this measurement model:

$$\theta \approx \alpha + \gamma \quad \text{and} \quad \beta \approx 0 \tag{41}$$

where γ is the flight path angle. This idea was previously implemented in UAV/MAV (Micro Aerial Vehicle) attitude determination, e.g., in Ref. 33. However, it is very common to make more assumptions such as the climb angle γ and the accelerations $[\dot{u},\ \dot{v},\ \dot{w}]^T$ to be zero. Consequently, this substantially reduces the allowed maneuvers to be performed by the UAV. If these assumptions are not adopted and we handle Eq. (39) it is possible to find analytical solutions for the Euler angles ϕ and θ. The solution for pitch measured angle $\theta_m = \theta$ can be obtained:

$$\theta_m = \arctan\left(\frac{a_1 a_2 \pm A_x\sqrt{a_1^2 + a_2^2 - A_x^2}}{A_x^2 - a_1^2}\right) \tag{42}$$

with

$$a_1 = -V_a\dot{\theta}\cos\gamma + V_a\dot{\gamma}\cos\gamma + V_a q\cos\gamma + \dot{V}_a\sin\gamma + g$$
$$a_2 = -V_a\dot{\gamma}\sin\gamma + V_a\dot{\theta}\sin\gamma - V_a q\sin\gamma + \dot{V}_a\cos\gamma$$

The solution for the roll measured angle $\phi_m = \phi$ can be derived as well:

$$\phi_m = \arcsin\left((-A_y - V_a r(c_\theta c_\gamma + s_\theta s_\gamma) + V_a p(s_\theta c_\gamma - c_\theta s_\gamma)/(g c_\theta)\right) \tag{43}$$

The measured yaw/course angle ψ_m can be obtained with the GPS velocity, as for the previous measurement model, Eq. (28), taking advantage of its relatively high precision. As happened with the Measurement Model 1, the current measurement model also runs on GPS availability. So, this measurement model has the Euler angles as measurements as well, where the vector $\underline{z}$ is given by:

$$\underline{z} = \begin{bmatrix} \phi_m \\ \theta_m \\ \psi_m \end{bmatrix} = \begin{bmatrix} \arcsin\left((-A_y - V_a r(c_\theta c_\gamma + s_\theta s_\gamma) + V_a p(s_\theta c_\gamma - c_\theta s_\gamma)/(g c_\theta)\right) \\ \arctan\left(\frac{a_1 a_2 - A_x\sqrt{a_1^2 + a_2^2 - A_x^2}}{A_x^2 - a_1^2}\right) \\ \arctan\left(\frac{v_{GPS_m}}{u_{GPS_m}}\right) \end{bmatrix} \tag{44}$$

This measurement model also works in *cascade*: the pitch angle θ_m is firstly calculated, then the ϕ_m can be calculated. The yaw angle can be calculated as desired. The Observation matrix of the Kalman filter is linear and given by Eq. (38) as well.

IV Results

In this section, the estimation results are presented. The derived algorithms (EKF_1 with measurements model 1 and EKF_2 with measurements model 2) were tested with computer simulated flights and then, the algorithm that attained best results tested with real flight data.

IV.A Simulation Flight Results

The fixed-wing UAV model used is based on the Aeronautical Simulation MATLAB/Simulink library. This library includes the *Aerosonde* UAV, a long-range weather-reconnaissance autonomous airplane, that was used as simulation model.

In order to properly simulate the developed algorithm, the characteristics of the sensors used in the simulation have the noise and bias values presented in Table 1. The Gauss-Markov gyroscopes parameters have the following values:[34] $\sigma_{b_w} = 211$ deg/h and $\tau_c = 382$ s.

Table 1 Noise and bias introduced in the simulation sensors.

	Symbol	Value
Accelerometer noise	σ_a	0.02 m/s^2
Gyroscope noise	σ_w	0.05 deg/s
Gyroscope *turn-on* bias	b_0	1.5 deg/s
Gyroscope bias stability	σ_{b_w}	211 deg/h
GPS velocity noise	$\sigma_{V_{GPS}}$	0.01 m/s
Airspeed noise	σ_{V_a}	0.06 m/s

The outputs of the IMUs and GPS were considered to provide measurements at rates equal to 100 Hz and 10 Hz, respectively. A particular situation should be noticed and taken in consideration. After rolling an angle ϕ about the X-axis of the aircraft, the angle of attack will have projections on both the new Y and Z-axis.[35] Thus, a *sideslip* β_{roll} appears and can be determined as follows:

$$\beta_{roll} = \arcsin(\sin\alpha\sin\phi) = \arcsin(\sin(\theta - \gamma)\sin\phi) \tag{45}$$

where the relation $\theta \approx \gamma + \alpha$ was used.

IV.A.1 Tuning Parameters

The tuning parameters of the EKF have to be properly defined in order to perform a good estimation. The process noise covariance matrices Q (6×6 matrix) can be defined as:

$$Q = diag\left(\left[\sigma_w^2,\ \sigma_w^2,\ \sigma_w^2,\ \frac{2\sigma_{b_w}^2}{\tau_c},\ \frac{2\sigma_{b_w}^2}{\tau_c},\ \frac{2\sigma_{b_w}^2}{\tau_c}\right]\right)$$

Due to the analytical solutions obtained for the measurements model, the measurements noise covariance matrices R (3×3 matrix) do not have a straightforward formulation as the process noise covariance matrices Q. Considering a standard deviation of $\sigma_\phi = \sigma_\theta = \sigma_\psi = 1$ deg for all the Euler angles:

$$R = diag\left(\left[\sigma_\phi^2,\ \sigma_\theta^2,\ \sigma_\psi^2\right]\right) \tag{46}$$

An investigation to verify if a Gaussian distribution still fits the measurements error/noise was performed and it confirmed that the distributions remain relatively Gaussian even under the nonlinear transformations/calculations of the measurements models. These results also provided a fair initial starting point to achieve the final R matrix.

Finally, regarding the characteristics of the bias of the gyroscopes it might be desirable to increase the convergence speed of their estimation.[2] Recall Eq. (25), from the KF process modeling, that can also be written as:

$$G\left[\underline{x}(t), t\right] = \begin{bmatrix} F_{x_{(1:3,4:6)}} & 0_{3\times3} \\ 0_{3\times3} & \lambda I_{3\times3} \end{bmatrix} \tag{47}$$

where the parameter λ was introduced and $F_{x_{(1:3,4:6)}}$ corresponds to a part of Jacobian of the process equations. It is possible to change the bias estimator poles by changing λ. In order to increase the speed of convergence due to the highly dynamic behavior of the UAVs it was chosen that:

$$\lambda = 10 \tag{48}$$

IV.A.2 Flight Results

One of the flights performed by the UAV has its 3D trajectory presented in Figure 1. A general flight was performed where the airplane turns right pitching up for a while and then turns left and starts descending varying its airspeed. The sideslip reaches moderate values in order to test the limits of the algorithm (Figure 2).

The estimated attitude angles of the UAV and the differences between the truth and estimation for both algorithms (EKF_1 and EKF_2) are presented respectively in Figures 3(a) and 3(b). As it is possible to see, the estimation error is relatively small during all simulation time: below 2 degrees for the all the Euler angles. Additionally, it is possible to notice the

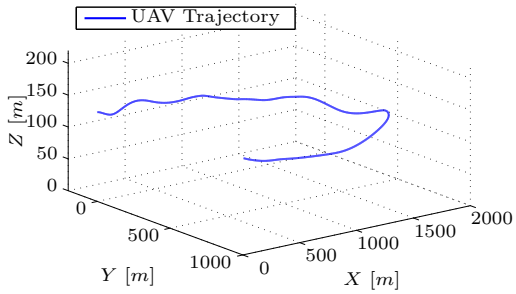

Fig. 1 3D position of simulated flight. Initial position: [0, 0, 40]m.

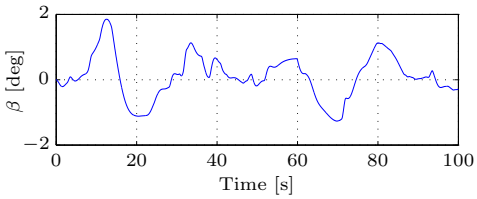

Fig. 2 Sideslip of simulated flight.

initial convergence for the three Euler angles. The numerical results of this flight are presented in Tables 2 and 3 where we can confirm these small estimation errors. The estimation performance for the yaw angle ψ is very similar for both algorithms due to same measurement update method used. Furthermore, the estimation errors are correlated with the sideslip angle (compare, for instance, the yaw angle estimation error in Figure 3(b) and the sideslip in Figure 2: when the sideslip angle increases, the yaw estimation error is higher). There is also a certain degree of correlation between the roll angle error for the EKF_2 and the sideslip angle.

Table 2 Numerical results of EKF_1

State Error	Mean	Std. Deviation
ϕ	-0.039 deg	0.135 deg
θ	-0.024 deg	0.136 deg
ψ	-0.150 deg	0.759 deg
b_p	0.027 deg/s	0.124 deg/s
b_q	-0.001 deg/s	0.094 deg/s
b_r	0.022 deg/s	0.165 deg/s

Table 3 Numerical results of EKF_2

State Error	Mean	Std. Deviation
ϕ	-0.080 deg	0.704 deg
θ	0.005 deg	0.355 deg
ψ	-0.160 deg	0.751 deg
b_p	-0.046 deg/s	0.349 deg/s
b_q	-0.030 deg/s	0.250 deg/s
b_r	0.030 deg/s	0.170 deg/s

IV.B Real Flight Results

The EKF_1 algorithm, with GPS-derived accelerations, was tested with real data. The application to real flight data is the ultimate test to an algorithm. A *MTi-G Xsens* device was used to collect the real data. It can provide us the *raw* data necessary to apply the derived attitude estimation algorithm. This

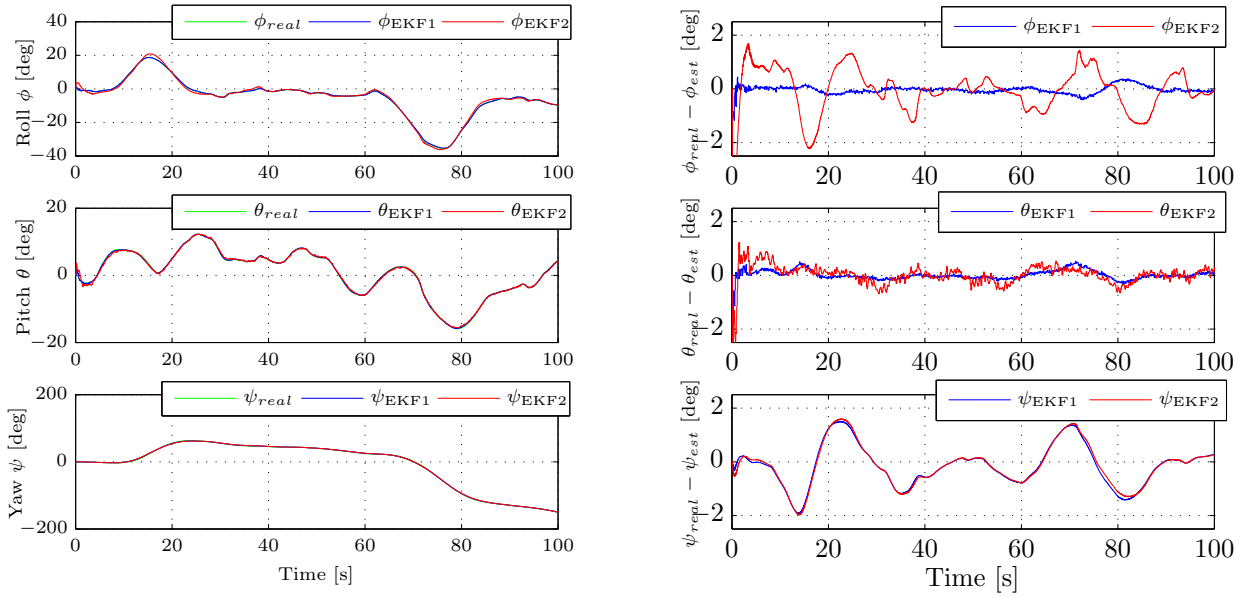

a) Estimation of ϕ, θ and ψ.

b) Differences between real and estimated angles.

Fig. 3 Estimated states for the simulation flight for EKF_1 and EKF_2.

device also estimates various position, velocity and attitude parameters, which includes the roll, pitch and yaw angles. The flight was performed on 2010-10-13 at Delft, The Netherlands, and a post-processing of the data was conducted. The utilized UAV is highly dynamic, performing wide maneuvers in few seconds. Figure 4 shows the *Easystar* UAV, used to obtain the flight data.

Fig. 4 Easystar UAV with 1.4m wingspan and 0.68kg of (empty) weight.

The lack of information about the inertial sensors of the MTi-G Xsens device makes the modeling of the sensors more difficult. However, this issue can be overcome by assuming the bias of the gyroscopes as presented in Eq. (18).

When multiple sensors are used, each producing its own data, synchronization among all the systems is required. The 1 Pulse-Per-Second (PPS) GPS signal provided by the MTi-G device was utilized to synchronize both navigation systems where all the data were aligned to GPS-time. Additionally, with the default configuration, the MTi-G outputs the data of the inertial sensors at a frequency of 100Hz and GPS measurements at 4Hz.

The real flight consists in highly dynamic maneuvers performed by the small UAV, constituted mainly by 360 degrees turns at constant altitude (see Figures 5 and 6). The GPS velocity of the aircraft varied approximately between 12 and 18m/s. The estimation algorithm runs while the aircraft is in the air ($t \in [44.12,\ 171.22]$s of the *log-file*) and no GPS outages were found.

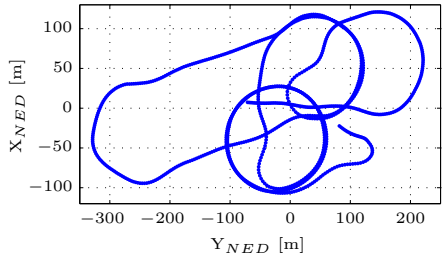

Fig. 5 North-East position provided by GPS.

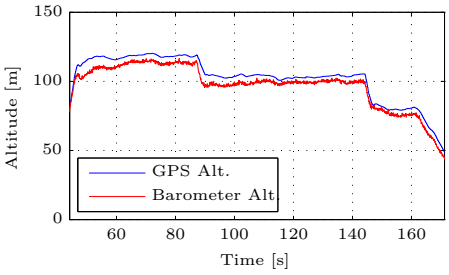

Fig. 6 Altitude provided by GPS and Barometer.

The estimated attitude angles, roll ϕ, pitch θ and yaw ψ can be seen in Figure 7. Since no information about the *real* attitude angles is available, the estimated Euler angles provided by the MTi-G Xsens device is also included for a matter of comparison.

We can see a consistent attitude tracking for all the angles. The roll angle is highly dynamic where we can notice wide maneuvers of almost 90 degrees (from

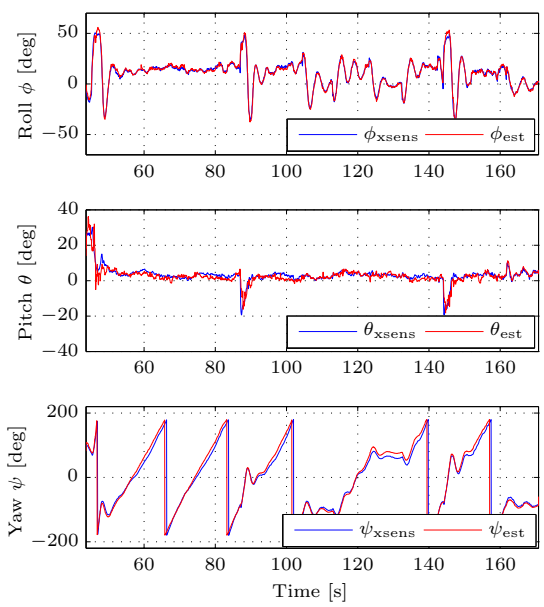

Fig. 7 Results of EKF$_1$ for real flight: Estimation of ϕ, θ and ψ.

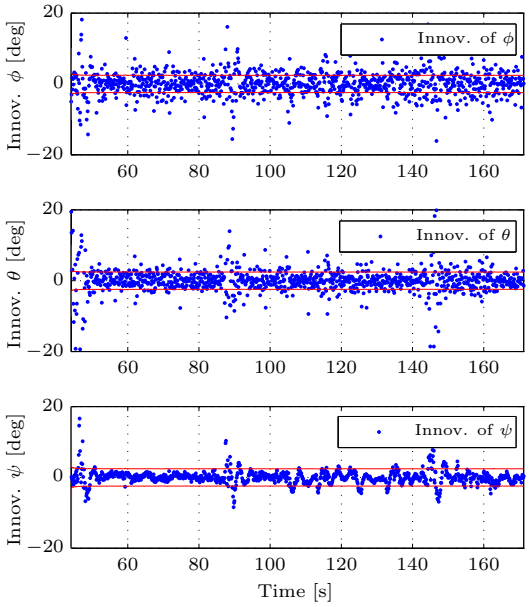

Fig. 8 Innovation sequences. The red line represents the standard deviation of the innovation.

$\phi \approx 50$deg to $\phi \approx -40$deg) in just 1.6 seconds (check $t \approx 88$s or $t \approx 166$s). Nevertheless, the algorithm seems to accomplish this fast attitude estimation without major difficulties. The pitch angle is consistent with an almost horizontal flight with two fast *pitch down* at $t = 87$s and $t = 144$s. The yaw angle estimation shows that the UAV performed several complete turns. We can also notice the fast initial convergence of the EKF.

In Figure 7, we can additionally observe angles estimated by the MTi-G Xsens device. Comparison between the two estimations let us conclude that they present small deviations between each other. Nevertheless, the yaw angle seems to exhibit some kind of *offset*. Since the MTi-G unit uses more instruments to estimate the attitude (such as magnetometers) it might be related to the sideslip angle. Small and light UAVs like this one can fly during long periods with high sideslip angles. However, since no true states are available we can not know which estimation algorithm is closer to the true yaw angle. In Table 4 the differences between the two estimations are presented. It is noticeable the similar performances of the roll and pitch estimations.

The best way to evaluate the performance of the EKF when no true states are available is by assessing the innovation sequences. Figure 8 shows the innovation sequences and their numerical results are presented in Table 5. They show an average close to zero and standard deviations around 4 degrees. Additionally, it was possible to confirm that the innovation sequences have a similar behavior to the ones obtained in the simulations: the roll and pitch estimations present a more *white* sequence and the yaw a more correlated one.

As a matter of curiosity, a particular aspect of the

Table 4 Numerical results: comparison of EKF$_1$ algorithm and MTi-G device.

State Error	Mean [deg]	Std. Deviation [deg]
ϕ	-0.118	2.083
θ	0.547	2.211
ψ	-5.788	8.273

Table 5 Innovation sequences of EKF$_1$.

Innovation	Mean [deg]	Std. Deviation [deg]
ϕ	0.046	3.636
θ	0.033	4.139
ψ	0.109	3.928

EKF algorithm is its estimation speed[4]. The time required to estimate the three attitude angles and the bias of the gyroscopes for the complete flight ($t_{\text{flight}} = 127.10$s) was only 0.569 seconds. The time average of each iteration was $t = 0.122$ms without GPS update and $t = 0.213$ms with measurements update.

V Conclusions

The work developed in this paper concerned the derivation of GPS/MEMS-INS (GPS/MEMS-AHRS) integration algorithms that would provide a fast, efficient and reliable attitude estimation for small highly dynamic UAVs. Two algorithms were developed and they make use of GPS-derived accelerations and airspeed sensors. The measurements equations of the correction steps of the EKF were analytically solved.

Concerning the simulation results, the *Half* EKFs with nonlinear process models and linear measurements models resulted in relatively small estimation errors but, overall, the EKF$_1$ demonstrated a better

[4]The computer specifications where the EKF$_1$ algorithm ran are: Intel Core^{TM} 2 Duo CPU T9550 2.66GHz with 4Gb RAM-Memory and Windows Vista Operating System.

performance than the EKF_2. The best attitude estimation was attained for the roll and pitch angles of the EKF_1 with 0.13 degrees of standard deviation of the error between the true and estimated angles. The yaw angle accuracy was confirmed to degrade upon flight situations where sideslip was present. However, even in more demanding situations that went beyond the algorithm assumptions, the estimation accuracy was not heavily decreased.

The EKF_1 algorithm was tested with real UAV flight data in a post-processing method. The algorithm demonstrated a consistent attitude tracking for all the Euler angles. Comparison of EKF_1 attitude estimation with the one provided by the MTi-G Xsens device showed that they are mainly in accordance with innovation sequences of the algorithm verifying its reliability.

References

[1]Caron, F., Duflos, E., Pomorski, D., and Vanheeghe, P., "GPS/IMU Data Fusion Using Multisensor Kalman Filtering: Introduction of Contextual Aspects," *Information Fusion*, Vol. 7, No. 2, 2006, pp. 221 – 230.

[2]Gebre-Egziabher, D., Hayward, R., and Powell, J., "Design of Multi-sensor Attitude Determination Systems," *Aerospace and Electronic Systems, IEEE Transactions on*, Vol. 40, No. 2, 2004, pp. 627 – 649.

[3]Kim, J., Sukkarieh, S., and Wishart, S., "Real-time Navigation, Guidance, and Control of a UAV using Low-cost Sensors," *Field and Service Robotics*, Vol. 7, Springer, 2006, pp. 299 – 309.

[4]Schultz, C. E., *INS and GPS Integration*, Master's thesis, Technical University of Denmark, Lyngby, 2006.

[5]Sarris, Z., "Survey of UAV Applications in Civil Markets," *The 9th IEEE Mediterranean Conference on Control and Automation*, Croatia, June 2001, p. 11.

[6]Barbour, N. M., "Inertial Navigation Sensors," *NATO RTO Lecture Series*, Vol. 232, 31 May - 1 June 2004.

[7]Gleason, S. and Gebre-Egziabher, D., *GNSS Applications and Methods*, Artech House Publishers, 2009.

[8]Shin, E.-H., *Estimation Techniques for Low-Cost Inertial Navigation*, Ph.D. thesis, Dept. of Geomatics Eng., University of Calgary, Calgary, Canada, 2005.

[9]Cheng, L., Zhaoying, Z., and Xu, F., "Attitude Determination for MAVs Using a Kalman Filter," *Tsinghua Science and Technology*, Vol. 13, No. 5, October 2008, pp. 593 – 597.

[10]Gebre-Egziabher, D., Klkaim, G. H., Powell, J., and Parkinson, B. W., "A Gyro-Free Quaternion-Based Attitude Determination System Suitable for Implementation Using Low Cost Sensors," *Proceedings of the IEEE Position, Location, and Navigation Symposium*, March 2000, pp. 185 – 192.

[11]Li, Y., Dempster, A., Li, B., Wang, J., and Rizos, C., "A Low-cost Attitude Heading Reference System by Combination of GPS and Magnetometers and MEMS Inertial Sensors for Mobile Applications," *Journal of Global Positioning Systems*, Vol. 5, 2006, pp. 88 – 95.

[12]Hayward, R., Gebre-Egziabher, D., Schwall, M., Powell, J., and Wilson, J., "Inertially Aided GPS Based Attitude Heading Reference System for General Aviation Aircraft," *Proceedings of the Institute of Navigation ION-GPS Conference*, 1997, pp. 1415 – 1424.

[13]Gebre-Egziabher, D., Hayward, R. C., and Powell, J. D., "A Low Cost GPS/Inertial Attitude Heading Reference System (AHRS) for General Aviation Applications," *Proceedings of the IEEE Position Location and Navigation Symposium, PLANS 1998*, 1998, pp. 518 – 525.

[14]Kornfeld, R. P., Hansman, R. J., and Deyst, J. J., "Single-antenna GPS-based aircraft attitude determination," *Navigation*, Vol. 45, No. 1, 1998, pp. 51 – 60.

[15]Gebre-Egziabher, D. and Elkaim, G., "MAV attitude determination by vector matching," *Aerospace and Electronic Systems, IEEE Transactions on*, Vol. 44, No. 3, 2008, pp. 1012 – 1028.

[16]Psiaki, M. L., Powell, S. P., and Kintner, P. M., "The Accuracy of the GPS-derived Acceleration Vector, A Novel Attitude Reference," *Proceedings of AIAA 1999 Guidance, Navigation, and Control Conference*, Portland, OR, August 1999, pp. 751 – 760.

[17]Schmidt, G. T. and Phillips, R., "INS/GPS Integration Architectures," *NATO RTO Lecture Series 232*, 5, October 2003, pp. 1 – 15.

[18]Brown, A. and Lu, Y., "Performance Test Results of an Integrated GPS/MEMS Inertial Navigation Package," *Proceedings of ION GNSS 2004*, September 2004, pp. 825 – 832.

[19]Welch, G. and Bishop, G., "An Introduction to the Kalman Filter," Tech. rep., Department of Computer Science, University of North Carolina, Chapel Hill, NC, 1995.

[20]Grewal, M. S., Weill, L. R., and Andrews, A. P., *Global Positioning Systems, Inertial Navigation, and Integration*, John Wiley & Sons Inc., 1st ed., 2001.

[21]Simon, D., *Optimal State Estimation: Kalman, H(infinity), and Nonlinear Approaches*, Wiley Interscience, 1st ed., 2006.

[22]Abdel-Hafez, M., "On the Development of an Inertial Navigation Error-budget System," *Journal of the Franklin Institute*, Vol. 348, Elsevier, 2009, pp. 24 – 44.

[23]Xing, Z. and Gebre-Egziabher, D., "Modeling and Bounding Low Cost Inertial Sensor Errors," *IEEE/ION PLANS 2008*, Monterey, CA, May 2008, pp. 1122 – 1132.

[24]Machado, F. M. R., *UAV State Determination based on the MEMS-IMU/GPS Loosely Coupled Integration*, Master's thesis, Faculdade de Engenharia da Universidade do Porto, Porto, Portugal, 2011.

[25]Premerlani, W. and Bizard, P., "Direction Cosine Matrix IMU: Theory," Available: http://gentlenav.googlecode.com/files/DCMDraft2.pdf.

[26]Kaplan, E. D. and Hegarty, C., *Understanding GPS Principles and Applications*, Artech House, Boston, MA, 2nd ed., 2006.

[27]Chalko, T. J., "High accuracy speed measurement using GPS (Global Positioning System)," Tech. rep., Scientific Engineering Research P/L, Mount Best, Victoria, Australia, 2007.

[28]Serrano, L., Kim, D., and Langley, R. B., "A GPS Velocity Sensor: How Accurate Can It Be? A First Look," *ION NTM 2004*, San Diego, California, 26 - 28 January 2004, pp. 875– 885.

[29]Psiaki, M. L., "Global Navigation Satellite Systems: Genesis, State of the Art, and Future Directions," *Plenary Presentation at the 46th Israel Annual Conference on Aerospace Sciences*, Tel Aviv and Haifa, Israel, March 2006.

[30]Pinder, S. D., Crowe, T. G., and Nikiforuk, P. N., "Application of the Global Positioning System in Determination of Vehicular Acceleration," *AIAA JAircraft*, Vol. 38, 2001, pp. 856 – 859.

[31]Lopes, H. J. D., *Attitude Determination of Highly Dynamic Fixed-wing UAVs*, Master's thesis, Delft University of Technology, Delft, The Netherlands, August 2011.

[32]Kingston, D. B., *Impremention Issues of Real-time Trajectory Generation on Small UAVs*, Master's thesis, Brigham Young University, 2004.

[33]Eldredge, A. M., *Improved State Estimation for Miniature Air Vehicles*, Master's thesis, Brigham Young University, 2006.

[34]Godha, S., *Performance Evaluation of Low Cost MEMS-Based IMU Integrated with GPS for Land Vehicle Navigation Application*, Master's thesis, The University of Calgary, Canada, 2006.

[35]Etkin, B. and Reid, L. D., *Dynamics of Flight: Stability and Control*, John Wiley & Sons, Inc., 1996.